Direct Observation of Transient Structural Dynamics of Atomically Thin Halide Perovskite Nanowires

Mengyu Gao[1,2], Yoonjae Park[3], Jianbo Jin[3], Peng-Cheng Chen[3,5], Hannah Devyldere[1], Yao Yang[3], Chengyu Song[4], Zhenni Lin[1,2], Qiuchen Zhao[3], Martin Siron[1,2], Mary C. Scott[1,4,*], David T. Limmer[2,3,*], and Peidong Yang[1,2,3,5,*]

1 Department of Materials Science and Engineering, University of California, Berkeley, Berkeley, California 94720, United States

2 Materials Sciences Division, Lawrence Berkeley National Laboratory, Berkeley, California 94720, United States

3 Department of Chemistry, University of California, Berkeley, Berkeley, California 94720, United States

4 National Center for Electron Microscopy, Molecular Foundry, Lawrence Berkeley National Laboratory, Berkeley, California 94720, United States

5 Kavli Energy NanoScience Institute, Berkeley, California 94720, United States

* Corresponding authors. E-mail: mary.scott@berkeley.edu (M.C.S), dlimmer@berkeley.edu (D.T.L), p_yang@berkeley.edu (P.Y.)

Abstract

Halide perovskite is a unique dynamical system, whose structural and chemical processes happening across different timescales have significant impact on its physical properties and device-level performance. However, due to its intrinsic instability, real-time investigation of the structure dynamics of halide perovskite is challenging, which hinders the systematic understanding of the chemical processes in the synthesis, phase transition, and degradation of halide perovskite. Here we show that atomically thin carbon materials can stabilize ultra-thin halide perovskite nanostructures against otherwise detrimental conditions. Moreover, the protective carbon shells enable atomic-level visualization of the vibrational, rotational, and translational movement of halide perovskite unit cells. Albeit atomically thin, protected halide perovskite nanostructures can maintain their structural integrity up to an electron dose rate of 10,000 $e^{-}/ Å^{2}\cdot s$, while exhibiting unusual dynamical behaviors pertaining to the lattice anharmonicity and nanoscale confinement. Our work demonstrates an effective method to protect beam sensitive materials during *in situ* observation, unlocking new solutions to study new modes of structure dynamics of nanomaterials.

Main text

Introduction

Understanding and visualizing dynamical processes in halide perovskite on relevant timescales is essential for fundamental knowledge and technological applications of this emerging optoelectronic material.[1–5] It has been shown that in halide perovskite lattice fluctuations due to large ionic framework and stereochemically active electron lone pairs could contribute to the intriguing electronic properties, such as dynamical dielectric screening.[6–9] On a longer timescale, structural transformations such as ionic transport and phase transitions have led into new applications beyond conventional optoelectronics.[10–13] Although the high ion diffusivity and rich phase diagrams of halide perovskite are manifestation of the vitality of the halide perovskite chemistry, these structural features also overshadow the commercialization of perovskite-based devices that demands long term stability. Whereas the importance of the dynamical

characteristics of halide perovskite has been well appreciated, an atomic-level investigation affording temporal information is still missing.

In recent years, *in situ* transmission electron microscopy (TEM), equipped with high-speed electron camera, has been recognized as a powerful tool to capture real-time dynamics at single-particle level.[14,15] With the sub-angstrom resolution imaging capability, *in situ* TEM could resolve local, irreversible structural dynamics that are usually beyond the reach of conventional laser spectroscopy, though the later has a much better time resolution.[16,17] However, one of the most critical limitations of using the high-speed electron camera to visualize fast chemical processes is its high electron dose rate; the minimal dose rate to achieve angstrom-level resolution in a single image at millisecond time resolution is around 5,000 $e^{-}/ Å^{2}\cdot s$,[18,19] which is well above the tolerance level of biological, organic molecules, and some inorganic materials, such as halide perovskite.[20–23] Moreover, to investigate nanoscale chemical processes or local inhomogeneity in a material, it is necessary to thin the material to the length scale of interest, which inevitably makes beam damage more pronounced.[24] Therefore, atomic resolution imaging using *in situ* TEM is typically limited to beam-tolerant materials, such as carbon allotropes[25,26] or metallic nanoparticles,[27–29] or reveals only slower dynamics.[30] Because of the demanding dose condition, there has been few *in situ* TEM studies on halide perovskite with high temporal and spatial resolution.[31,32]

To address this problem, we develop a system that comprises of carbon nanotube-encapsulated single-unit-cell thick halide perovskite nanowires, suspended on graphene TEM grids. The perovskite nanostructures synthesized with this method are remarkably stable under various conditions (humidity, heating, and electron flux), therefore enabling us to directly observe structural dynamics of a soft semiconductor lattice within an *in situ* TEM. Due to the strong geometrical confinement, the atomically thin 1D perovskite nanowires exhibit local and correlative structural dynamics that are overlooked by conventional characterizations techniques.

Results and discussion

Static structural characterization. Single-unit-cell thick Cs-Pb-I nanowires were isolated with the spatial confinement of single-walled carbon nanotubes, whose diameter is roughly 1.2-1.4 nm (**Figure 1**). The samples were cleaned and annealed on TEM grids with suspended monolayer graphene. Since halide perovskites are sensitive to multiple environmental stimuli,

such as humidity, heating, and high-energy electron beams, which poses an obstacle to the direct synthesis and investigation of ultrathin perovskite objects, in this study we highlight the utilization of atomically thin carbon materials, with critical improvement over previous approaches,[25,33–35] to overcome these difficulties (synthetic and post-processing details are described in the **Supporting Information**). Firstly, the single-walled carbon nanotubes provide a flexible scaffold to synthesize atomically thin 1D perovskite nanowires with high crystallinity and stability against electron beams, polar environment, and heating. The atomic-level confinement also enables the growth of new structures beyond typical synthetic methods. Secondly, the nanowires are supported on monolayer graphene, which provides an e-beam transparent substrate while sufficiently stabilizing and separating nanowire bundles so that imaging an individual wire with atomic resolution is possible. Thirdly, because both graphene and carbon nanotubes are stable and protective against heating and polar solvents, we can clean the perovskite crystals grown outside the nanotubes with polar solvents and anneal the TEM grids under high temperature to remove carbon contaminations. Using this approach, we obtain ultraclean systems with desirable yield of the products for systematic investigation (**Figure S1-2**). This approach is also applicable to synthesize and observe other 1D or 2D inorganic materials with atomic level precision (**Figure S5, and S19**).

Conventional (S)TEM characterization techniques were used to identify the structure and phase of 1D perovskite nanowires. Fast Fourier transform (FFT) patterns of the high-resolution (S)TEM images have confirmed the lattice constant of the 1D perovskite to be 0.61-0.63 nm, comparable to nearest lead to lead distance in 3D $CsPbI_3$ phase (**Figure S9 and S21**). Interestingly, contrary to the bulk $CsPbI_3$, whose thermodynamically stable phase at room temperature is edge-shared, non-perovskite δ-phase,[36] at atomically thin 1D geometry, the stable phase is corner-shared perovskite phase. We also observed the coexistence of both α-phase and δ-phase in thicker nanowires, indicating the effect geometrical confinement as an alternative method[37–39] on stabilizing the photoactive perovskite phase (**Figure 1B, and Figure S19**). The chirality of carbon nanotubes could be simultaneously determined (**Figure S9-10**), which is used for later theoretical calculations in this study. Correlated energy-dispersive X-ray spectrum (EDS) of the imaged structure show the presence of all three elements, though atomic resolution elementary mapping is impractical given its high electron dose requirement and the dynamicity of the atomically thin structure (**Figure S3-4**). From both ADF-STEM and BF-TEM images we

have identified two typical orientations of the perovskite lattice. Compared with an ideal cubic perovskite lattice, these two orientations resemble the atom arrangement viewed from [100] and [110] directions (**Figure 1C** and **D**). Even though the periodic structure of the nanowires resembles the perovskite lattice, structural distortion is obvious. Instead of having a cubic unit cell, the unit cell of the nanowires has a contracted cesium framework and an expanded iodine framework. We estimate the lattice contraction to be roughly 10% and the expansion to be roughly 15% compared with an ideal cubic perovskite structure (**Figure S20**).

Besides the two typical crystallographic zone axes observed in different wires as mentioned above, some interesting but unexpected features also emerged during the acquisition. For example, we captured nanowires whose different segments display two orientations simultaneously (**Figure 1E, Figure S6**). As typically STEM takes seconds for the electron beam to scan across the sample, the observed nanowire *twisting* might either due to the intrinsic torsional instability of 1D octahedral structure[40] or because the nanowires were rotating during the acquisition time window. In fact, we observed that for the same nanowire, the STEM images vary from scan to scan, and even the orientation of a nanowire changes from [100] to [110] (**Figure 1F**). Both observations imply that the 1D perovskite nanowires inside carbon nanotubes are not trivial structures categorized as ordinary low-dimensional perovskite. Moreover, the dynamical details of the 1D perovskite are likely overlooked by slow acquisition methods, such as STEM. The atoms or even the segments of nanowires undergo constant motion, leaving blurred or even missing contrast in the acquired images. We also attempted to use atomic electron tomography (an angstrom-level technique based on the reconstruction of multiple titling-series images[41,42]) to resolve the 3D structure of the nanowires, but only to find that the reconstructed structure showed no atomic-level features (**Figure S11, S12**). The difficulties by employing techniques with slow probes to target at atomic resolution necessitate the re-evaluation of the structural understanding of atomically thin perovskite and a proper technique to capture the intriguing dynamics.

Real-time observation of transient structural dynamics. In this regard, we switched to use transmission electron microscopes equipped with spherical aberration correctors (to remove lens distortion), an electron monochromator (to improve the beam's energy coherence), and a high-efficiency (quantum efficiency > 85%) direct electron detection camera (to count almost every electron and to achieve high time resolution). Because of the stability of the encapsulated

nanowires, a wide range of electron dose rate (from 100 to 10,000 $e^{-}/ Å^{2}\cdot s$) can be applied to achieve both atomic resolution and high frame rate (5 to 40 milliseconds per frame), while the sample integrity is maintained throughout the acquisition. The atomic sample thinness enables us to use phase contrast mode to unambiguously resolve atomic structures with time resolution unreachable by STEM (**Figure 2A**). Taking advantage of the time resolution and reliable contrast interpretation, atom tracing algorithm was performed to track the time trace of every atom column in the nanowire segments. The coordinates of atom columns and the atom species were determined for every frame in our time series acquisition, and thereafter we could recover the dynamical behaviors of the perovskite nanowires. These dynamical behaviors were divided into two modes (**Figure S13**), one local, the other collective. The local mode of dynamics resolves the motion of atoms in single unit cells, while the collective mode derives from the collative motions of atoms in a nanowire segment.

For the local dynamics, we profiled how the individual perovskite frameworks distort and vibrate around their equilibrium positions (**Figure 2B**). From the trajectories of cesium and iodine atoms, we observed that the cesium atoms are relatively stable, and the fluctuation of their coordinates is isotropic; however, spatial distributions of iodine atoms are more anisotropic compared with cesium atoms (**Figure 2C**). The bridging iodine atoms in the center line of the nanowire are more mobile than the terminating iodine atoms at the edges of the nanowire. Two types of iodine atoms, owing to their different dynamical behaviors, even exhibit different contrasts in the ADF-STEM images, where the bridging sites have lower contrast compared with terminating sites, a phenomenon that sometimes appears in the HR STEM images of perovskite nanostructures but has received little attention. Owing to the different coordination environments of the iodine atoms we observed a more distorted iodine framework compared with the framework composed of cesium atoms. We used the stretching and bending normal modes of a square as a basis to decompose the cesium and iodine frameworks and analyzed their distribution throughout the 5-second time frame. Within this time scale, more than 100 frames were analyzed, and the corresponding distortions were decomposed based on 7 possible symmetry modes pertaining to a square framework (**Figure S17**). As shown in **Figure 2D**, the amplitudes of the third distortion component, corresponding to the asymmetric stretching mode (inset of **Figure 2D**), of cesium atoms are distributed symmetrically around zero, which means their stretching on average sustain the square symmetry. On the other hand, the medium of the

amplitudes of iodine atoms are away from zero, and the distributions are no longer symmetric. This quantitative difference in their distortion modes demonstrates the anisotropic nature of the lattice dynamics of different atoms in the atomically thin 1D system.

In addition to local atomic distortion, we also studied the motion of a whole nanowire segment. We tracked the trajectories of the center atom column in the unit cell, whose coordinates were taken to be the pivot point representing the motion of the unit cell (**Figure 3A**). From the ensemble of the coordinates, a correlative mode of motion is identified: the whole segment of a nanowire is moving inside a carbon nanotube. The collective motion is not due to the drifting of the grid support or the vibration of the nanotube, because we have properly removed the sample drifting by a cross-correlation algorithm, and we have also observed different motion directions in different nanotubes in the same field of view. Interestingly, the collective motion of the nanowire segments is not totally random. In fact, drastic jumps were observed to be interlaced in a relatively stable regime (**Figure 3B**). The translational motion of a solid-state material inside ultrathin carbon nanotubes is a unique case among the studies of liquid-carbon quantum friction in 1D confinement.[43,44]

Besides the translational collective motion, we also captured nanowire rotation *in situ*. As discussed earlier, when using STEM, the orientation of the nanowires could change during scanning. With the fast electron camera and atom tracing algorithm, we now investigate the nanowire rotation with a better time resolution. For a nanowire segment, we found that the contrast line scan of the center line is shifted by half of the unit cell length (**Figure 4AB, Figure S15-16**), which is because when the nanowire is oriented along [100], the brightest atom contrast is attributed to the I-Pb-I column, while when viewed along [110], the brightest atom contrast is attributed to the Cs-I-Cs column. Because of the rotation from [100] to [110], the terminating halide will move closer to the center of the unit cell, while the cesium atoms on the corner of the unit cell will move away from the centerline of the nanowire. We tracked the trajectories of the atom contrast in a single unit cell (**Figure 4C**) and overlaid the trajectories to demonstrate the real-time observation of the nanowire rotation (**Figure 4D**). The direct observation of nanowire rotation points to the intrinsic octahedral instability of perovskite,[6] especially when octahedral coordination constraints are relieved in lower dimensionalities.

Structural resilience of single-unit-cell thick halide perovskite nanowires. To quantify the structural dynamics of 1D perovskite nanowires, we adopted a definition of the Lindemann parameter as an order parameter to describe the spatial distribution of the unit cells: $L_D^i(\Delta t) = \left\langle x_{t+\Delta t}^i - x_t^i \right\rangle^2 / a^2$, where i denotes the i^{th} unit cell, Δt is the time interval between the two time frames, and a is the averaged distance between center atoms, which is then defined as the lattice constant. In principle, the Lindemann parameter is zero when Δt is zero, and it reaches a plateau when Δt approaches infinity. In the time scale of our acquisition (10 to 30 seconds), we assume $L_D^i(\Delta t)$ reaches its plateau and is thus Δt independent. Now the analysis of the Lindemann parameter $L_D^i = \lim_{\Delta t \to \infty} L_D^i(\Delta t)$ can be considered as a quantitative descriptor to characterize the local or global structural distortion. The dynamical structure for a segment is then characterized by the averaged Lindemann constant $L_D = 1/N \sum_i L_D^i$, where N is the number of unit cells. Equipped with the atom tracing technique and quantification methods, we conducted dose dependent studies (**Figure 3C**) to understand the structural transition of the robust 1D system under electron beams. With increased electron doses (from 2,000 to 15,000 $e^-/Å^2 \cdot s$), it is found that the Lindemann constant for the nanowires increases but is still below the extent to which structural melting could happen (when L_D is approaching 0.1). Even though the order parameter (L_D) nanowire segment is below the Lindemann melting criteria, some of the unit cells have reached a much higher local Lindemann constants, indicating the presence of local defects (**Figure 3A**, **Figure S14**), which casts doubts on ensemble characterization methods where local information is averaged or simply overlooked.

The local and collective motions observed here have their origin in the intrinsic softness of halide perovskite and the strong electron-matter interaction under the imaging condition. But on the other hand, the dynamical lattice observed here is also quite resilient towards the electron beams, given the highest electron dose rate used in our experiments reached 10,000 $e^-/ Å^2 \cdot s$, with an accumulated dose more than 500,000 $e^-/ Å^2$. No phase separation or loss of mass were observed unless a defect was found in the nanotube. For a typical halide perovskite nanostructure, however, even an accumulated dose of 1,000 $e^-/ Å^2$ will destroy the structure. The strong spatial confinement of nanotubes mitigates the knock-on damage, while the presence of carbon nanotubes and graphene can effectively conduct electrons and heat, which are major mechanisms for beam damage.

Molecular dynamics simulation. To support the analysis on the underlying structure and dynamics of perovskite nanowires in carbon nanotubes, we performed molecular dynamics simulations of a simple empirical model.[45] We find that carbon nanotubes with a diameter of 1.39 nm stabilizes the octahedral structure of the one-dimensional chain. The stoichiometry of the perovskite nanowire studies was Cs_3PbI_5, where a Cs^+ vacancy is introduced for charge neutrality. A characteristic snapshot of the simulation is shown in **Fig. 5A**. Analogous to the inferences from the TEM images, the simulations illustrate highly anisotropic fluctuations of the atoms along the nanowire. This is quantified by evaluating the distributions of distances between a central lead atom and the neighboring cesium, bridging, and terminating iodine atoms (**Fig. 5B).** In agreement with the experiment, the fluctuations away from equilibrium distance for cesium atoms and terminating iodine atoms are relatively symmetric whereas the distribution of bridging iodine atoms has a tail due to the stretching motions of Pb-I, consistent with that in **Fig. 2C**.

Motivated by the rotations of the nanowire captured experimentally, we also analyzed the angle, Θ, between a Pb-I unit vector $\mathbf{R}_{\text{Pb-I}}$ in a unit cell and another Pb-I unit vector in an adjacent unit cell $\mathbf{R}'_{\text{Pb-I}}$ using the relation of $\cos(\Theta) = \mathbf{R}_{\text{Pb-I}} \cdot \mathbf{R}'_{\text{Pb-I}}$. **Figure 5C** shows the representative time series of these angles, which shows that the unit cell routinely rotates by roughly 90° and the rotation occurs in the timescale of few ns, much slower than the expected vibrational timescale for atoms. To characterize the timescale of rotations, we computed time auto-correlation function $C(t)$ of $\mathbf{R}_{\text{Pb-I}}$, defined as $C(t) = \langle \mathbf{R}_{\text{Pb-I}}(t) \cdot \mathbf{R}_{\text{Pb-I}}(0) \rangle$. **Figure 5D** illustrates $C(t)$ for both types of iodides where the correlation related to bridging iodides does not decay due to the fixed Pb-I-Pb orientation whereas the correlation associated with terminating iodides slowly decays, indicating that the source of the loss of correlation is from rotations of individual unit cells. Such rotations are thermally accessible in part due to the distortions around the Cs^+ vacancies. Static evidence of rotations is clear from the probability density of atoms in a unit cell using coordinates projected onto the plane along the nanowire. Shown in **Fig. 5E** is the probability density of iodine atoms and cesium atoms where x and y axes represent the direction along and perpendicular to the nanowire. The broad density of cesium atoms implies the rotation of unit cell and the contraction in cesium framework observed in the experiments can be attributed to slightly shorter Cs-Cs distance near the edges.

Concluding remarks

The comprehensive spatiotemporal description of 1D perovskite nanowires under strong confinement has directly revealed the unprecedented dynamical behaviors of nanostructured halide perovskite that evade conventional characterization and understanding. The resilience of the structural fluctuations protected by ultrathin carbon materials against the polar environment, heating, and impinging electron flux suggests a new route for quantitative studies of the structural transformation (such as phase transition or ion diffusion) of low-dimensional systems which are otherwise vulnerable to external stimuli.

Supporting information

The Supporting Information is available free of charge at xxxxxxx-xxxxxxx

Description of experimental details, image processing and atom tracing algorithms, additional characterization data, simulation details, including atomic resolution (S)TEM images, tomographic reconstruction data, electron energy dispersive spectroscopy and mapping, TEM simulation, videos of real time imaging of structural dynamics of a single-unit-cell thick perovskite nanowire.

Acknowledgements

The authors thank Dr. P. Ercius, Dr. J. Ciston, Dr. Y. Zhang, Dr. J. Ondry, and Dr. S. Louisia for technical support. **Funding**: This work was supported by the U.S. Department of Energy, Office of Science, Office of Basic Energy Sciences, Materials Sciences and Engineering Division, under Contract No. DE-AC02-05-CH11231 within the Fundamentals of Semiconductor Nanowire Program (KCPY23). J.J. acknowledges fellowship support from Suzhou Industrial Park. P.-C.C. acknowledges support from Kavli ENSI Heising-Simons Fellowship. Y.Y. acknowledges support from Miller Fellowship. **Data and materials availability**: The datasets generated during and/or analyzed during the current study are available from the corresponding authors on reasonable request.

References

1. Stranks, S. D. Multimodal microscopy characterization of halide perovskite semiconductors: Revealing a new world (dis)order. *Matter* **4**, 3852–3866 (2021).
2. Gao, M. *et al.* The making of a reconfigurable semiconductor with a soft ionic lattice. *Matter* **4**, 3874–3896 (2021).
3. Buizza, L. R. V. & Herz, L. M. Polarons and Charge Localization in Metal-Halide Semiconductors for Photovoltaic and Light-Emitting Devices. *Adv. Mater.* **2007057**, 1–19 (2021).
4. Miyata, K. *et al.* Large polarons in lead halide perovskites. *Sci. Adv.* **3**, e1701217-10 (2017).
5. Munson, K. T. & Asbury, J. B. Influence of Dynamic Disorder and Charge–Lattice Interactions on Optoelectronic Properties of Halide Perovskites. *J. Phys. Chem. C* **125**, 5427–5435 (2021).
6. Fu, Y., Jin, S. & Zhu, X. Y. Stereochemical expression of ns 2 electron pairs in metal halide perovskites. *Nat. Rev. Chem.* **5**, 838–852 (2021).
7. Puppin, M. *et al.* Evidence of Large Polarons in Photoemission Band Mapping of the Perovskite Semiconductor CsPbBr3. *Phys. Rev. Lett.* **124**, 206402 (2020).
8. Lanigan-Atkins, T. *et al.* Two-dimensional overdamped fluctuations of the soft perovskite lattice in CsPbBr3. *Nat. Mater.* **20**, 977–983 (2021).
9. Park, Y., Obliger, A. & Limmer, D. T. Nonlocal Screening Dictates the Radiative Lifetimes of Excitations in Lead Halide Perovskites. *Nano Lett.* **22**, 2398–2404 (2022).
10. Dou, L. *et al.* Spatially resolved multicolor CsPbX₃ nanowire heterojunctions via anion exchange. *Proc. Natl. Acad. Sci.* **114**, 7216 LP – 7221 (2017).
11. Shi, E. *et al.* Two-dimensional halide perovskite lateral epitaxial heterostructures. *Nature* **580**, 614–620 (2020).
12. Steele, J. A. *et al.* Phase Transitions and Anion Exchange in All-Inorganic Halide Perovskites. *Accounts Mater. Res.* **1**, 3–15 (2020).
13. Bischak, C. G. *et al.* Origin of Reversible Photoinduced Phase Separation in Hybrid Perovskites. *Nano Lett.* **17**, 1028–1033 (2017).

14. Zheng, H. *et al.* Observation of Single Colloidal Platinum Nanocrystal Growth Trajectories. *Science (80-.).* **324**, 1309–1312 (2009).

15. Ross, F. M. Opportunities and challenges in liquid cell electron microscopy. *Science (80-.).* **350**, (2015).

16. Zewail, A. H. 4D ultrafast electron diffraction, crystallography, and microscopy. *Annu. Rev. Phys. Chem.* **57**, 65–103 (2006).

17. Kraus, P. M., Zamp, M., Cushing, S. K., Neumark, D. M. & Leone, S. R. Time-resolved experimental techniques have played a major role in our fundamental understanding of chemical processes. Temperature jump. *Nat. Rev. Chem.* **2**, 82–94 (2018).

18. Lee, Z., Rose, H., Lehtinen, O., Biskupek, J. & Kaiser, U. Electron dose dependence of signal-to-noise ratio, atom contrast and resolution in transmission electron microscope images. *Ultramicroscopy* **145**, 3–12 (2014).

19. Rose, H. H. Future trends in aberration-corrected electron microscopy. *Philos. Trans. R. Soc. A Math. Phys. Eng. Sci.* **367**, 3809–3823 (2009).

20. Zhang, D. *et al.* Atomic-resolution transmission electron microscopy of electron beam–sensitive crystalline materials. *Science (80-.).* **359**, 675–679 (2018).

21. Yu, Y. *et al.* Atomic Resolution Imaging of Halide Perovskites. *Nano Lett.* **16**, 7530–7535 (2016).

22. Egerton, R. F., Li, P. & Malac, M. Radiation damage in the TEM and SEM. *Micron* **35**, 399–409 (2004).

23. Rothmann, M. U. *et al.* Structural and Chemical Changes to CH3NH3PbI3 Induced by Electron and Gallium Ion Beams. *Adv. Mater.* **30**, 1–7 (2018).

24. Billinge, S. J. L. & Levin, I. The problem with determining atomic structure at the nanoscale. *Science (80-.).* **316**, 561–565 (2007).

25. Koshino, M. *et al.* Analysis of the reactivity and selectivity of fullerene dimerization reactions at the atomic level. *Nat. Chem.* **2**, 117–124 (2010).

26. Shimizu, T., Lungerich, D., Harano, K. & Nakamura, E. Time-Resolved Imaging of Stochastic Cascade Reactions over a Submillisecond to Second Time Range at the Angstrom Level. *J. Am. Chem. Soc.* **144**, 9797–9805 (2022).

27. Fu, X., Chen, B., Tang, J., Hassan, M. T. & Zewail, A. H. Imaging rotational dynamics of nanoparticles in liquid by 4D electron microscopy. *Science (80-.).* **355**, 494–498 (2017).

28. Kim, B. H. *et al.* Critical differences in 3D atomic structure of individual ligand-protected nanocrystals in solution. *Science (80-.).* **368**, 60–67 (2020).

29. Jeon, S. *et al.* Reversible disorder-order transitions in atomic crystal nucleation. *Science (80-.).* **371**, 498–503 (2021).

30. Xiong, H. *et al.* In situ imaging of the sorption-induced subcell topological flexibility of a rigid zeolite framework. *Science (80-.).* **376**, 491–496 (2022).

31. Rothmann, M. U. *et al.* Atomic-scale microstructure of metal halide perovskite. *Science* **370**, (2020).

32. Dang, Z. *et al.* In Situ Transmission Electron Microscopy Study of Electron Beam-Induced Transformations in Colloidal Cesium Lead Halide Perovskite Nanocrystals. *ACS Nano* **11**, 2124–2132 (2017).

33. Meyer, R. R. *et al.* Discrete atom imaging of one-dimensional crystals formed within single-walled carbon nanotubes. *Science (80-.).* **289**, 1324–1326 (2000).

34. Algara-Siller, G., Kurasch, S., Sedighi, M., Lehtinen, O. & Kaiser, U. The pristine atomic structure of MoS2 monolayer protected from electron radiation damage by graphene. *Appl. Phys. Lett.* **103**, (2013).

35. Nakamuro, T., Sakakibara, M., Nada, H., Harano, K. & Nakamura, E. Capturing the Moment of Emergence of Crystal Nucleus from Disorder. *J. Am. Chem. Soc.* **143**, 1763–1767 (2021).

36. Straus, D. B., Guo, S. & Cava, R. J. Kinetically Stable Single Crystals of Perovskite-Phase CsPbI3. *J. Am. Chem. Soc.* **141**, 11435–11439 (2019).

37. Zhang, D. *et al.* Synthesis of Composition Tunable and Highly Luminescent Cesium Lead Halide Nanowires through Anion-Exchange Reactions. *J. Am. Chem. Soc.* **138**, 7236–7239 (2016).

38. Gao, M. *et al.* Scaling Laws of Exciton Recombination Kinetics in Low Dimensional Halide Perovskite Nanostructures. *J. Am. Chem. Soc.* **142**, 8871–8879.

39. Swarnkar, A. *et al.* Quantum dot–induced phase stabilization of α-CsPbI3 perovskite for

high-efficiency photovoltaics. *Science (80-.).* **354**, 92–95 (2016).

40. Pham, T. *et al.* Torsional instability in the single-chain limit of a transition metal trichalcogenide. *Science (80-.).* **361**, 263–266 (2018).

41. Scott, M. C. *et al.* Electron tomography at 2.4-ångström resolution. *Nature* **483**, 444–447 (2012).

42. Chen, P.-C. *et al.* Revealing the Phase Separation Behavior of Thermodynamically Immiscible Elements in a Nanoparticle. *Nano Lett.* **21**, 6684–6689.

43. Keerthi, A. *et al.* Ballistic molecular transport through two-dimensional channels. *Nature* **558**, 420–423 (2018).

44. Kavokine, N., Bocquet, M. L. & Bocquet, L. Fluctuation-induced quantum friction in nanoscale water flows. *Nature* **602**, 84–90 (2022).

45. Plimpton, S. Fast Parallel Algorithms for Short-Range Molecular Dynamics. *J. Comput. Phys.* **117**, 1–19 (1995).

Figures

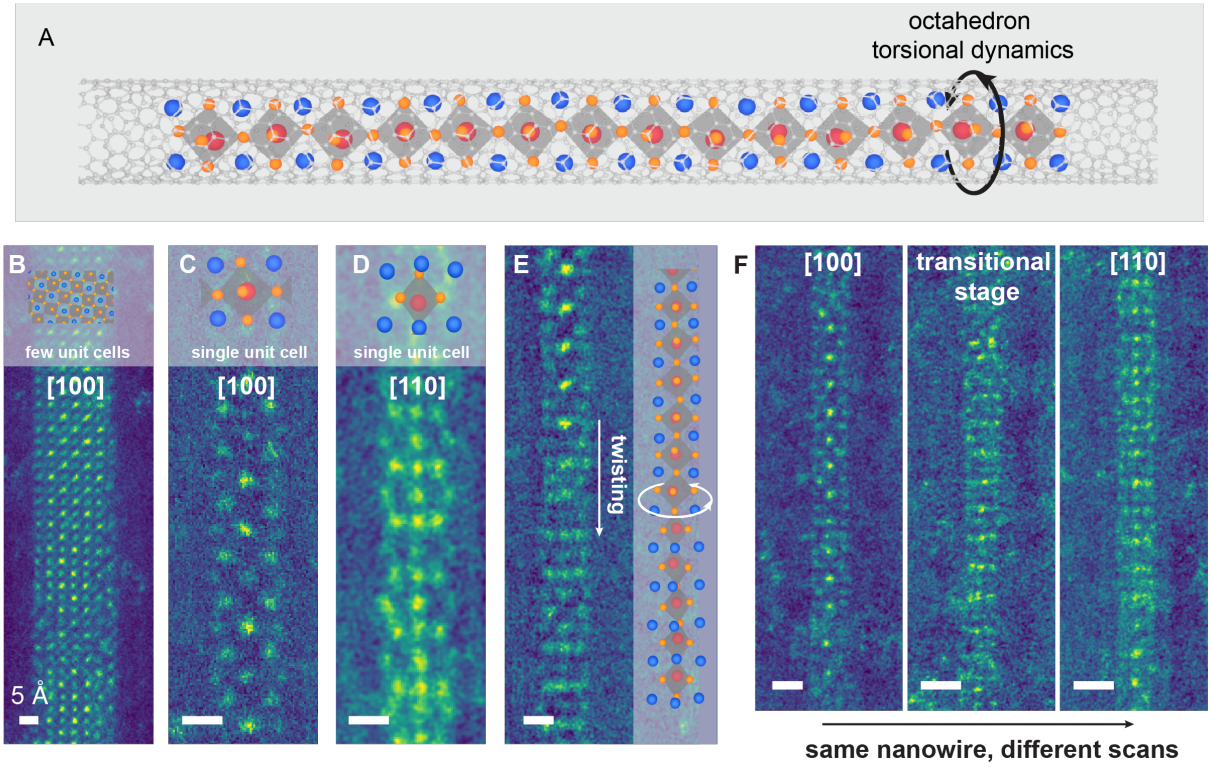

Figure 1 | ADF-STEM characterization of the static structure of atomically thin Cs-Pb-I nanowires. (A) Schematic model of 1D perovskite nanowires confined in single-walled carbon nanotubes. Red: lead atoms; orange: iodine atoms; blue: cesium atoms. Typical ADF-STEM images of 1D perovskite nanowires in diameters and different crystallographic orientations. (B) Few-unit-cell α-phase $CsPbI_3$ perovskite nanowire viewed along [100], with a growth direction of [011], and single-unit-cell nanowires (C) viewed along [100], (D) viewed along [110], and (E) a peculiar observation that within a single nanowire two segments display two different crystallographic orientations. (F) Structural change of the same nanowire during different scans. The scanning positions of three images are slightly different due to the sample drifting during the acquisition. Scale bars: 5Å.

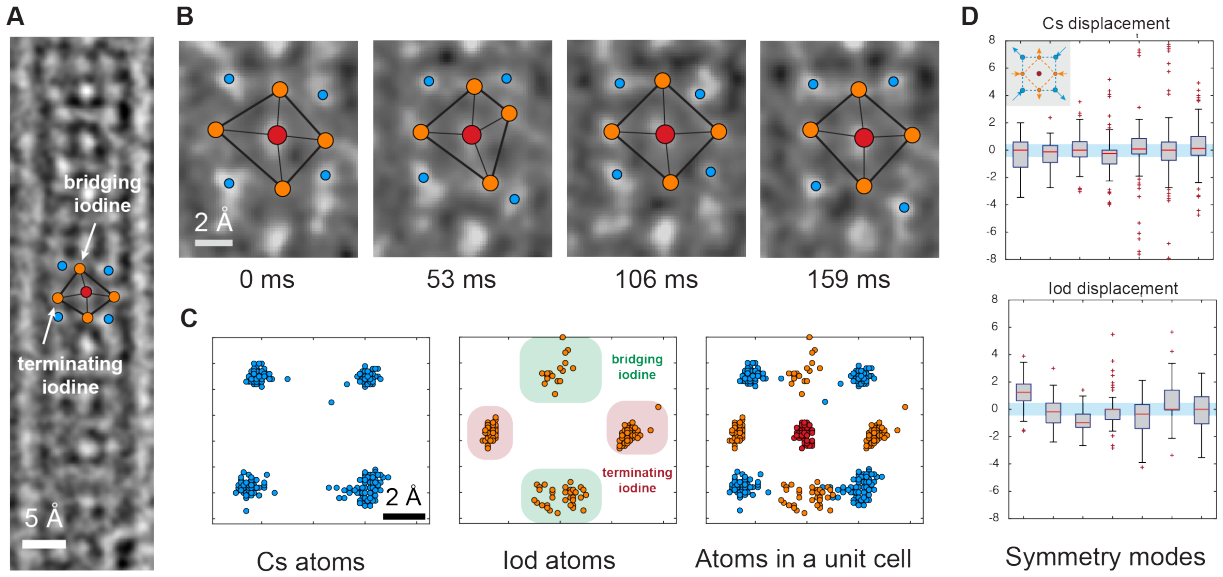

Figure 2 | Transient structural distortion of individual octahedral units. (A) Representative atomic-resolution TEM image of a segment of the nanowire. (B) Time-series of TEM images of a single unit cell in the nanowire. (C) Real time trajectories of cesium (blue), lead (red), and iodine (orange) atoms within the 5-second timeframe (time interval is 53 millisecond). (D) Unit-cell framework distortion of cesium and iodine decomposed based on 7 symmetry modes of a square. Inset shows the asymmetric stretching mode, whose amplitudes are shown in column three.

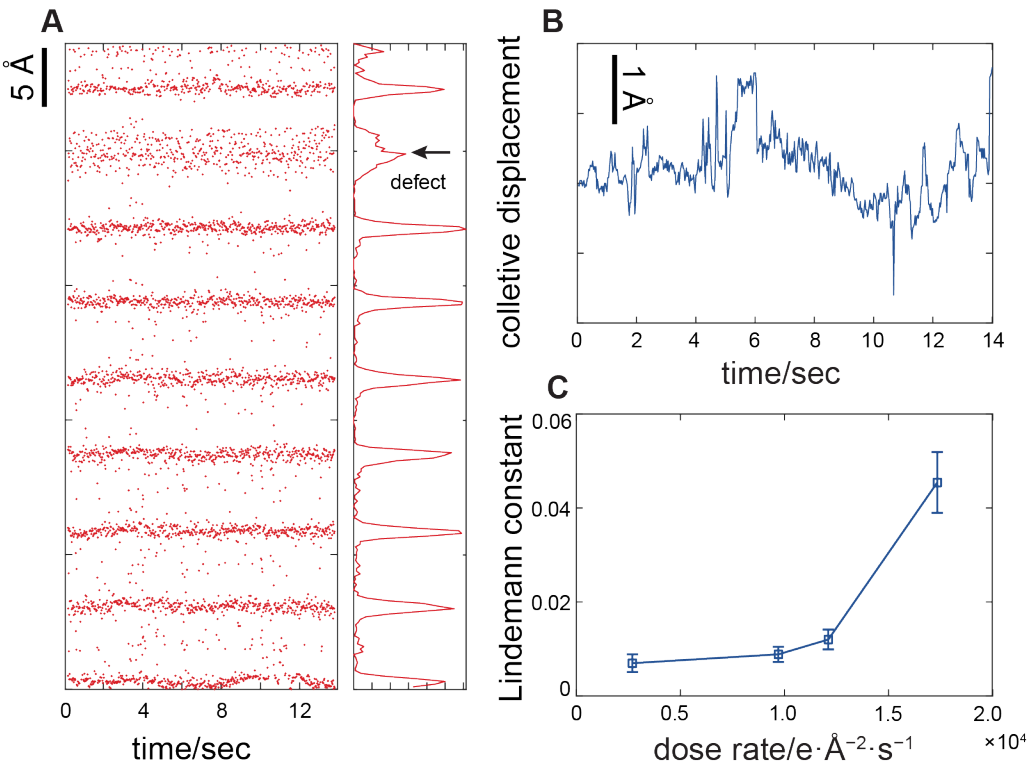

Figure 3 | Real-time characterization of the unit cell displacement and collective motion. (A) Real-time coordinates of unit cell centers and the histogram of the coordinates. The collective motion of the whole segment of the nanowire is decoupled from the trajectory tracing. The blue arrow points to an atom column whose spatial distribution is more dynamical than others'. (B) Real-time tracking of the collective displacement of the whole segment of the nanowire. (C) Dose dependent experiments where the coordinates of the unit cells are used to calculate the order parameter Lindemann constant as a function of electron doses. The total time elapsed for each dose experiment is typically around 10 seconds.

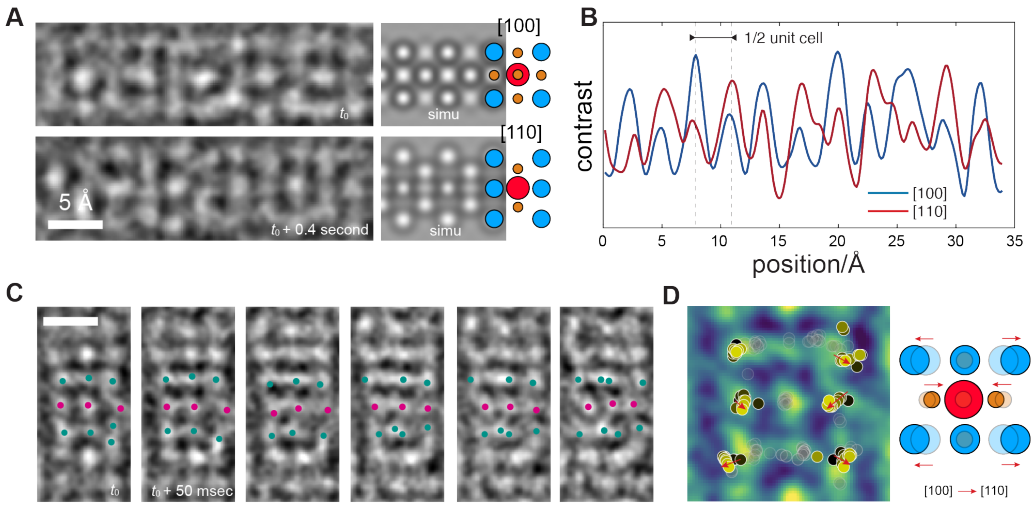

Figure 4 | *In situ* nanowire rotation. (A) Two real-time snapshots of the same nanowire segment separated by 0.4 second. The images are averaged with 8 frames taken at frame rate of 20 frames per second. (B) Contrast line scan along the centerline of the nanowire segment shown in (A). (C) Individual frames for the same nanowire shown in (A). (D) Trajectories of atoms overlaid to show the twisting effect. Scale bars: 5Å.

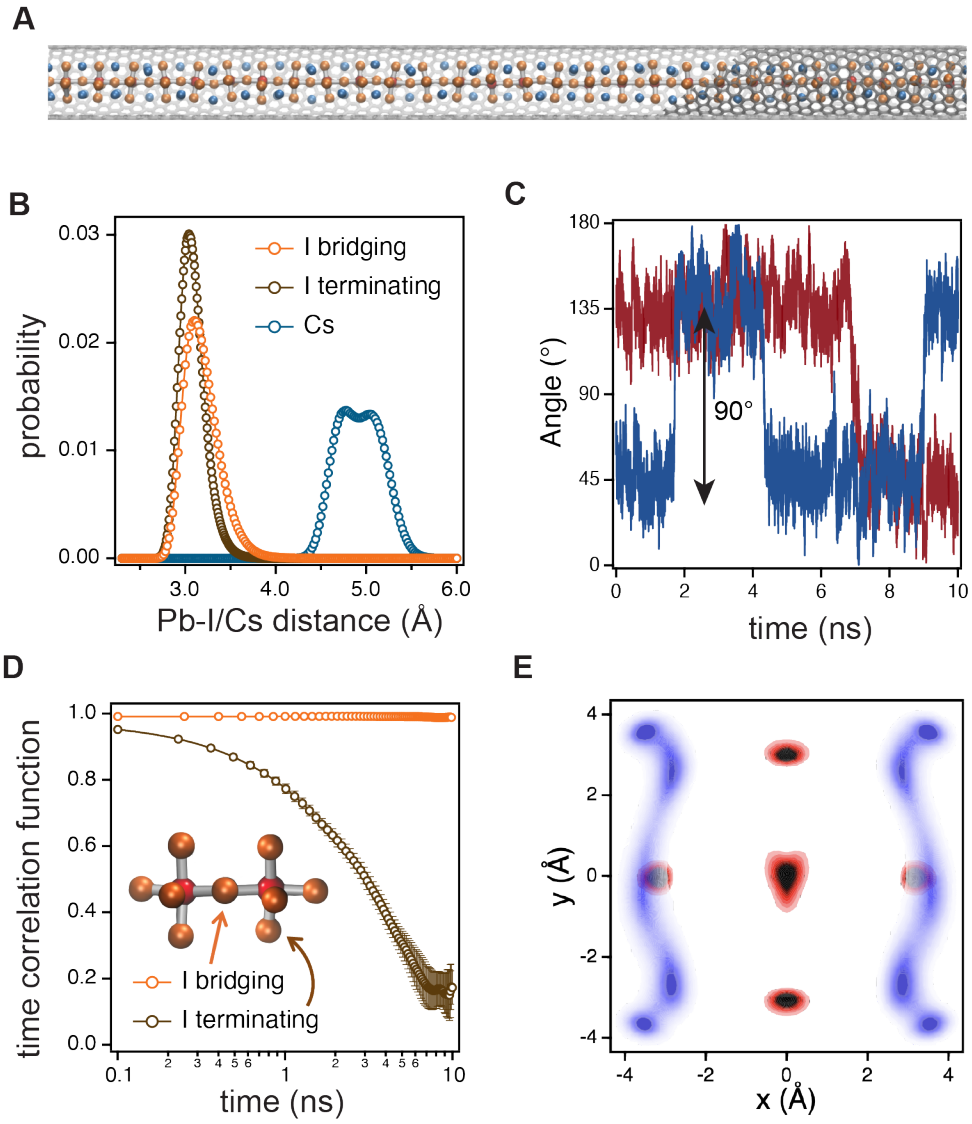

Figure 5 | Molecular dynamics simulation of the 1D perovskite nanowires confined in single walled carbon nanotubes. (A) Snapshot of simulation on perovskite nanowire in carbon nanotubes where red, orange, and blue atoms represent Pb^{2+}, I^{-}, and Cs^{+}. (B) Probability distribution of the distance between center lead atom and cesium atoms (blue symbols), bridging iodine atoms (orange symbols), and terminating iodine atoms (brown symbols) in a unit cell. (C) Representative time series of angles Θ between neighboring $\mathbf{R}_{Pb\text{-}I}$ vectors. (D) Time auto-correlation function of $\mathbf{R}_{Pb\text{-}I}$ for bridging (orange symbols) and terminating (brown symbols) iodine atoms. (E) Probability density of atoms projected onto the plane along the nanowire for iodine atoms (red) and cesium atoms (blue) within a unit cell where darker color indicates higher density.

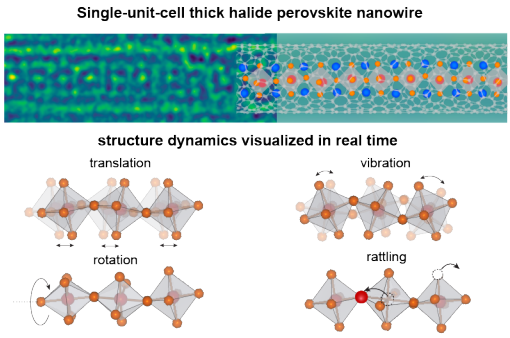

Figure for Table of Contents